The intraoperative relationship between intracochlear electrical field and excitability of the auditory nerve

Söderqvist, Samuel

2022-12

Söderqvist , S , Sinkkonen , S T & Sivonen , V 2022 , ' The intraoperative relationship between intracochlear electrical field and excitability of the auditory nerve ' , Heliyon , vol. 8 , no. 12 , e11970 . https://doi.org/10.1016/j.heliyon.2022.e11970

http://hdl.handle.net/10138/354058
https://doi.org/10.1016/j.heliyon.2022.e11970

Heliyon 8 (2022) e11970

Contents lists available at ScienceDirect

Heliyon

journal homepage: www.cell.com/heliyon

Research article

The intraoperative relationship between intracochlear electrical field and excitability of the auditory nerve

Samuel Söderqvist *, Saku T. Sinkkonen, Ville Sivonen

Department of Otorhinolaryngology – Head and Neck Surgery, Head and Neck Center, Helsinki University Hospital and University of Helsinki, Helsinki, Finland

HIGHLIGHTS

- Intracochlear electrical field peak amplitude and width had an inverse relationship with eCAP thresholds.
- In large cochleae, the intracochlear electrical field peak amplitudes were shallower than in small cochleae.
- Intracochlear electrical fields with a high peak amplitude were also wide-spreading along the electrode array.

ARTICLE INFO

Keywords:
Cochlear implant
Electrically evoked compound action potential
Intracochlear electrical field
Cochlear diameter

ABSTRACT

A limiting factor of cochlear implant (CI) technology is the electrode-contact overlapping spread of the electrode-generated intracochlear electrical field (EF). While the extent of the spread can be reduced with intracochlear ground electrodes, the stimulation level must be increased to reach similar loudness as with monopolar stimulation utilizing an extracochlear ground. In this study, we investigated the relationship between the monopolar intracochlear EF and the minimum stimulation level required for a measurable neural response assessed with electrically evoked compound action potential (eCAP) thresholds in intraoperative settings. Also, the effect of cochlear diameter on the intracochlear EF was evaluated, as narrower intracochlear EFs were found from larger than smaller cochleae in an earlier study.

A total of 171 ears of severely-to-profoundly hearing-impaired patients (ages 0.7–89 years; 42.5 ± 27.8 years, mean ± SD) implanted with a Cochlear Nucleus CI522 or CI622 implant and Slim Straight electrode array or with a Med-El Synchrony implant and Flex 28 electrode array were included in the study. Normal anatomy was established and cochlear diameter was measured for all patients from preoperative imaging. Intraoperative intracochlear EF and eCAP threshold measurements were measured for both Cochlear and Med-El devices with the CIs' back-telemetry options, and EF and eCAP were compared for Cochlear devices.

The peak and width of the intracochlear EF correlated with each other ($r = 0.46$, $p < 0.001$), and both had an inverse relationship with eCAP thresholds ($r = –0.41$, $p < 0.001$ and $r = –0.29$, $p < 0.001$, respectively). The peak amplitudes of the intracochlear EF increased towards the apical part of the electrode array with both Cochlear ($r = 0.97$, $p < 0.001$) and Med-El ($r = 0.80$, $p = 0.002$) devices. The peak amplitudes of the intracochlear EF were shallower across the electrode array in large than in small cochleae ($p < 0.05$).

Our results indicate that the responsiveness of the cochlear nerve is not only dependent on neural health but is also affected by the physical environment of the electrode array, which can be assessed by measuring the intracochlear EF. Further studies are warranted to investigate the detailed characteristics of the intracochlear current spread in CI recipients with varying anatomical features of the cochlea and with electrode arrays with different locations in the scalae or related to the modiolus in the cochleae.

* Corresponding author.
E-mail address: samuel.soderqvist@hus.fi (S. Söderqvist).

https://doi.org/10.1016/j.heliyon.2022.e11970
Received 30 June 2022; Received in revised form 10 October 2022; Accepted 22 November 2022

1. Introduction

A cochlear implant (CI) helps patients with severe-to-profound hearing loss to perceive sound and communicate verbally. However, when compared to normal hearing, CI recipients suffer from diminished spectral resolution and poorer speech recognition, especially in background noise (Dorman and Gifford, 2017). The auditory sensation with a CI is ultimately generated by directly stimulating the spiral ganglion neurons (SGNs) in the inner ear with an electrode array. Depending on the model, an electrode array consists of 12–22 separate electrode contacts, which is a strikingly low number when compared to about 3 500 rows of tonotopically organized hair cells inside the cochlea. In addition, because of the substantial overlap between the electrode-generated spread of intracochlear electrical fields (EFs), CI recipients perform as their electrode arrays would have ten or less independent channels (Friesen et al., 2001).

Several approaches have been taken over the years to reduce channel interaction in CIs. Shortly after the development of the multichannel CI, a processing strategy was pioneered to interleave the spectrum of the sound signal by stimulating electrode contacts sequentially. The aim of this so-called continuous interleaved sampling (Wilson et al., 1991) was to minimize electrical interaction between electrode contacts, and it forms the basis of the most commonly used CI sound coding still today. Later attempts focused on placing the electrode array as near to the SGNs as possible. Perimodiolar placement has been shown to result in narrower neural excitation profiles when compared to lateral placement of the electrode array within the same cochlea (Cohen et al., 2003). More recently, there has been growing interest in current focusing by using the intracochlear electrodes to ground the stimulating current. With tripolar stimulation, where the adjacent electrodes of the stimulating electrode are used as grounds and the current loop is entirely intracochlear, the spread of the EF can be reduced potentially achieving narrower patterns of stimulated SGNs and improved speech recognition in complex listening situations (Snyder et al., 2004; Srinivasan et al., 2013; Padilla and Landsberger, 2016; Luo and Wu, 2016). However, to reach similar loudness levels as with monopolar stimulation with an extracochlear ground, the stimulating current in tripolar stimulation must be significantly increased (Landsberger et al., 2012), potentially debilitating the beneficial effects of current focusing (Morris and Pfingst, 2000).

To effectively detect the malfunctioning of a CI, the manufacturers have developed objective back-telemetry tests for device function (Hey et al., 2015). These measurements include the ability to record voltages at individual electrode contacts in response to current flow to estimate channel impedances and the spread of the intracochlear EF. With the former, the majority of short and open circuits can be detected (Hughes et al., 2004). Also, abnormally high impedances might be seen after meningitis related intracochlear fibrous tissue growth around the electrode array and ossification of the cochlea (Durisin et al., 2015; Helmstaedter et al., 2018). High contact impedances at the basal electrodes may reveal electrode migration out of the cochlea (Dietz et al., 2016). Recordings of the EF are also used to assess more subtle abnormalities in the electrode array and its surroundings, such as tip fold-overs (Zuniga et al., 2017; Hoppe et al., 2022). With a complete insertion of the electrode array and without any cochlear pathologies, the most relevant patient-related factors affecting the intracochlear EF spread are believed to be cochlear dimensions and geometry (Bai et al., 2019; Lei et al., 2021), the placement of the electrode array (Shepherd et al., 1993), and the conductivity of the tissues in the ear (Briaire and Frijns, 2000; Nogueira et al., 2016).

The spread of the intracochlear EF is purely a physical measure and can be recorded in saline and from cadavers and plastic cochlea models (de Rijk et al., 2020; Swaddiwudhipong et al., 2020). Therefore, to make inferences about the effect of the EF on auditory perception, its relationship with psychophysical loudness as well as with patterns of neural activation has been studied. The intracochlear EF seems to be similar between the different manufacturers (Swaddiwudhipong et al., 2020), despite slight differences in the measurement methods. In Cochlear (Sydney, Australia) devices the voltage is recorded for each stimulating and recording electrode pair separately, while in Advanced Bionics (Valencia, CA, USA) and Med-El (Innsbruck, Austria) devices the EF distribution can be recorded simultaneously from all non-stimulated electrode contacts (Vanpoucke et al., 2004).

Berenstein et al. (2010) investigated loudness produced with monopolar stimulation and its combination with tripolar stimulation to estimate an effective field magnitude from the spread of intracochlear EF recordings. In EF measurements, the transimpedance recorded from the stimulating electrode includes a fast-decaying reactive component from the electrode-tissue interface and thus, Berenstein et al. (2010) assumed that the magnitude of the EF recorded at the stimulating electrode does not reach the neural components at its full potential. As it is impossible to record the transimpedance without the reactive component (effective transimpedance, Z_{eff}) at the location of the stimulating electrode, it has to be modeled based on the recordings from the rest of the electrodes (Berenstein et al., 2010) utilizing the knowledge of exponential decay of the intracochlear EF (Briaire and Frijns, 2000). Berenstein et al. (2010) found that loudness was determined by the Z_{eff}, and both loudness and the Z_{eff} increased with the stimulating current. In our earlier study (Söderqvist et al., 2021), we substituted the recorded transimpedance at the location of the stimulating electrode with a Z_{eff} to estimate an effective intracochlear EF (EF_{eff}), which allowed a more realistic comparison between the widths of the EF_{eff} and neural activation. We found that the profiles and widths of the EF_{eff} correlate with the patterns of the activated SGNs, as measured with the forward-masking paradigm for the spread of neural excitation.

Similarly, with impedance measurements, modern CIs can be used to record the excitability of the auditory nerve to electrical stimulation via the electrically evoked compound action potential (eCAP; Lai et al., 2002). The eCAP amplitude, defined as the potential difference between the negative and positive peaks in an eCAP recording, depicts the strength and synchrony of the SGN activation (Lai and Dillier, 2000). As the eCAP amplitude increases with the stimulating current, an amplitude growth function (AGF) can be determined and further used to extrapolate the current level that elicits an eCAP amplitude of zero (eCAP threshold). Another method to determine the eCAP threshold is to repeat the eCAP measurement with a stimulation level around the assumed threshold level, and inspect what is the lowest current causing a visible eCAP over ground-noise level. A low eCAP threshold indicates that the cochlear nerve (CN) is easily excitable with electrical stimulation, but its correlation with the behavioral stimulation levels is moderate at best (Morita et al., 2003; Cafarelli Dees et al., 2005; Miller et al., 2008; Jeon et al., 2010). In animal models, the ears with better SGN survival possess steeper AGF slopes when compared to ears with sparse SGN density (Pfingst et al., 2015; Colesa et al., 2021). Also, it seems that the AGF slope is unaffected by intrascalar tissue growth (Swiderski et al., 2020). However, a similar relationship between neural health and eCAP thresholds has not been established.

The eCAP can be reliably measured from over 90% of CI recipients (Cafarelli Dees et al., 2005; Cooper et al., 2020). However, there is a great intersubject variability in eCAP thresholds, which is not explained by age or either duration or etiology of deafness (Morita et al., 2003; Cafarelli Dees et al., 2005; Jahn and Arenberg, 2020). Also, in lateral-wall electrode arrays, the eCAP thresholds are dependent on the recording location and tend to increase from apical to basal direction, which is a consistent finding between studies (Cafarelli Dees et al., 2005; Telmesani and Said, 2015; Christov et al., 2019; Söderqvist et al., 2021). Further, both the eCAP and psychophysical threshold levels increase with the distance of an electrode from the modiolus (known as modiolar distance) or from the mid-modiolar axis (van Wermeskerken et al., 2009; Long et al., 2014; Davis et al., 2016; Mewes et al., 2020; Schvartz-Leyzac et al., 2020). The extent of neural activation is somewhat narrower in larger than in smaller cochleae (Söderqvist et al., 2021), which could be due to a larger volume of the scala tympani (ST) over which the intracochlear EF

decreases. On the other hand, a shallower decay of the intracochlear EF towards the apex has been detected in both modeling (Bai et al., 2019) and in vivo studies (Berenstein et al., 2010; Tang et al., 2011; Söderqvist et al., 2021), suggesting a physical background of the eCAP threshold variability at different sections of the electrode array.

The aim of this study was to investigate the relationship between the intracochlear EF in terms of peak amplitude (Z_{eff}) and width with the responsiveness of the CN estimated via eCAP thresholds. As the profiles of the EF and neural excitation correlate (Söderqvist et al., 2021), the peak amplitude of the effective EF is related to psychophysical loudness (Berenstein et al., 2010) and eCAP amplitudes and loudness increase monotonically with stimulation current (Kirby et al., 2012), our hypothesis was that when a wide intracochlear EF with a high peak amplitude is generated by the stimulating electrode, less current is required to elicit a measurable neural response. In addition to the relationship between intracochlear EF and eCAP thresholds, we also evaluated the effects of cochlear diameter and CI manufacturer on the peak amplitude of the intracochlear EF. As in earlier studies narrow EFs and high eCAP thresholds were associated with large cochleae (Söderqvist et al., 2021, 2022), we expected to find shallower EF peaks from larger than smaller cochleae.

2. Methods

2.1. Study design and ethics

This was a retrospective cohort study approved by the institutional review board of the Hospital District of Helsinki and Uusimaa. Due to the retrospective nature of the study, the ethical committee and informed consent were not required by the Finnish national legislation.

2.2. Subjects

The study subjects consisted of two cohorts. In the first cohort, there were 99 consecutive severely-to-profoundly hearing-impaired patients (40 males and 59 females; ages 0.7–89 years; 35.8 ± 26.6 years, mean ± SD) implanted with a Cochlear Nucleus CI522 or CI622 implant and Slim Straight electrode array between January 2019 and December 2021. Twenty-three of the patients were implanted bilaterally, resulting in 122 implanted ears. Three ears were excluded from further analysis due to incomplete insertion or an open circuit in monopolar impedance measurements. The second cohort consisted of patients implanted with a Med-El Synchrony implant and Flex 28 electrode array between January 2015 and December 2021. Seventy-four ears of 71 severely-to-profoundly hearing-impaired patients were implanted with a Med-El device (25 males and 49 females; ages 3.4–85.1 years; 60.5 ± 18.8 years, mean ± SD). The intraoperative EF recordings were available from all study subjects. The eCAP thresholds were analyzed only from the recipients of Cochlear devices, as eCAP recordings were found only for 16 out of 74 ears with Med-El devices. Further, only three out of twelve electrode contacts had ten or more eCAP thresholds recorded. All patients were operated with the round window approach at Helsinki University Hospital at the Department of Otorhinolaryngology – Head and Neck Surgery. The following information was gathered: the age at the time of the surgery, the etiology of hearing loss, the size of the cochlea measured from computed tomography (CT) images, and the existence of an identifiable cochlear nerve in preoperative magnetic resonance images. The details of the patient demographics are described in Table 1 in the Appendix.

2.3. Intraoperative recordings

The intraoperative spread of the EF and eCAP thresholds were recorded from Cochlear devices via the transimpedance matrix (TIM) and automated neural response telemetry (AutoNRT) using the extrapolation method with the Custom Sound EP software. For Med-El devices, the EF spread was recorded via impedance field telemetry (IFT) with the Med-El Maestro software. All measurements were made during the final stages of the CI surgery after wound closure when the patient was still under general anesthesia. Prior to TIM measurements, the electrode array was conditioned by sweeping the contacts with 25 μs wide pulses at 230 current level (CL) to decrease the contact impedances with electrical stimulation (Newbold et al., 2011). For TIM, a maximum CL that did not exceed 230 CL and did not result in out-of-compliance or saturation was used and this was 207 ± 12.7 (mean ± SD) CL with a pulse width of 25 μs. For IFT, the charge was always 0.5 nanocoulombs (nC) and the pulse width was 26.7 μs.

The eCAP thresholds were measured with a pulse width of 25 μs and a rate of 250 Hz via AutoNRT and determined automatically by the measurement software. The recording electrode was two contacts apically from the stimulating electrode, with an exception for the two most apical electrodes, whose stimulation were recorded two contacts basally. From 113 to 117 out of 119 NRT recordings were available from each electrode. Electrode specific details are found in Table 2 in the Appendix.

2.4. Effective intracochlear electrical field

In the vicinity of the stimulating electrode the intracochlear EF decreases rapidly and linearly (Briaire and Frijns, 2000) likely due to the electrode-tissue interface (Berenstein et al., 2010). Further away from the stimulating electrode, which was estimated to be 0.4 mm by Berenstein et al. (2010), the decay of the EF is exponential. This information was used to compute an effective transimpedance (Z_{eff}), which was thought to represent the transimpedance at the location of the neural tissue. In this study, the MATLAB (MathWorks, Natick, MA, USA) function *fminsearch* was used to model Z_{eff} and effective voltage (U_{eff}) based on the recorded values from the non-stimulated electrodes. These modeled values were used to substitute the corresponding monopolar value at the location of the stimulated electrode together with subtracting a dc offset from the modeled and recorded transimpedances to create an effective TIM (TIM_{eff}) or IFT (IFT_{eff}). Function *findpeaks,* which finds a peak from a curve and computes its width, was used with *halfheight* as reference to estimate their 50% widths in millimeters along the electrode array similarly to Söderqvist et al. (2021). Also, a dc offset was deducted from Z_{eff} and U_{eff} for further analysis.

Figure 1 illustrates examples of TIM and TIM_{eff} (Figure 1A) as well as IFT and IFT_{eff} (Figure 1B) with the corresponding 50% widths of the EF_{eff}s. The modeling was considered successful if Z_{eff} was between 0–2500 Ω, effective voltage (U_{eff}) between 0–1.5 V, TIM 50% width between 2–20 electrode contacts (1.82–18.2 mm), and IFT 50% width between 1–11 electrode contacts (1.93–21.23 mm). In total, 113–116 TIM_{eff} and 28–73 IFT_{eff} were modeled, as well as 109–116 TIM_{eff} 50% widths were estimated from each electrode contact, respectively. The electrode-specific details are in Table 2 in the Appendix. Due to fewer electrode contacts in the Med-El electrode arrays, only 0–69 % of the IFT_{eff} 50% widths were successfully computed (Table 2). Thus, the relationship between the IFT_{eff} peak amplitude and 50% width was not analyzed further.

2.5. Cochlear diameter and insertion angle

All patients were preoperatively imaged with a standard high-resolution computed tomography (CT) clinical protocol used in the Hospital District of Helsinki and Uusimaa. The diameter of the cochlea was evaluated by an otoradiologist from the reconstructed CT images of the cochlea as described by Alexiades et al. (2015). Even though the cochlea is a tapered structure, the cochlea diameter can be used to estimate the cochlear duct length with a linear equation (Alexiades et al., 2015). The mean ± SD cochlear diameters were 8.77 ± 0.35 and 8.81 ± 0.35 mm for Cochlear and Med-El groups, respectively.

To evaluate the effect of the cochlear diameter on the peak amplitude of the intracochlear EF, the ears were sorted into four groups according to

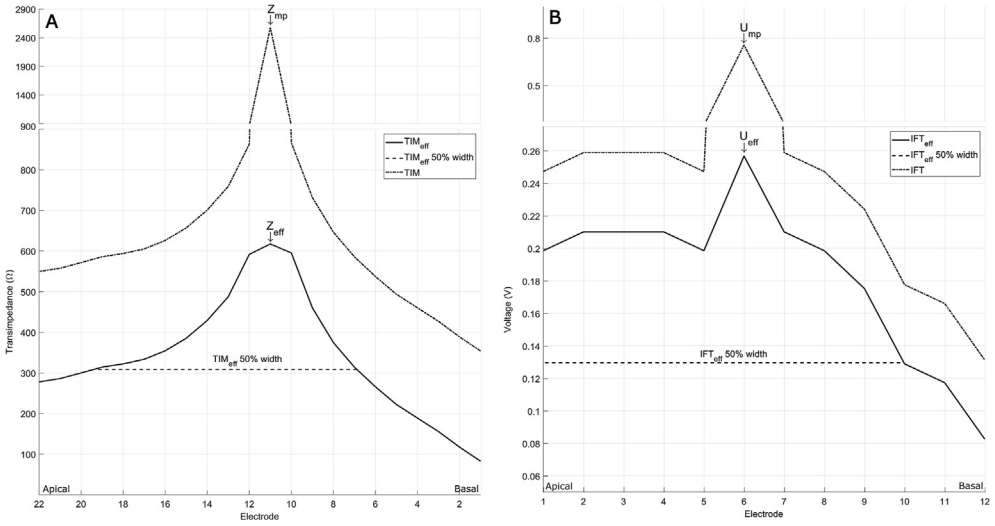

Figure 1. Examples of recorded and modeled intracochlear EFs, peak amplitudes, and 50% widths. The electrode contacts are arranged from the apical to basal direction. In contrast to recorded transimpedance matrix (TIM) and impedance field telemetry (IFT), in the effective TIM (TIM_{eff}) and IFT (IFT_{eff}), transimpedance (Z_{mp}) or voltage (U_{mp}) the recorded at the stimulating electrode was substituted with a modeled effective transimpedance (Z_{eff}) or voltage (U_{eff}) and a dc offset was deducted. A) The transimpedance matrix (TIM) was recorded from all 22 intracochlear electrodes. B) IFT was recorded from all 12 intracochlear electrodes.

their diameter. In the first group, the dimensions are less than –1 SD, in the second group between –1 SD and the mean, in the third group between the mean and +1 SD, and in the fourth group larger than +1 SD, resulting in 16, 39, 48, and 14 ears in each group, respectively.

To compare the spread of the intracochlear EF between Cochlear and Med-El devices, computational electrode insertion angles were applied in addition to the actual electrode numbers. Based on the patients' operative charts, all the CI electrode arrays were fully inserted through the round window route. The most basal electrode is located 5.0 and 4.9 mm from the full insertion mark and the following electrodes are separated with a distance of 0.91 and 1.92 mm in Slim Straight and Flex 28 electrode arrays, respectively. Therefore, the linear location of each electrode's basal edge (L in mm) was calculated using:

$$L = \textit{distance of the most basal electrode from the full insertion mark} + \textit{distance between electrodes} \times (\textit{electrode number} - 1)\ \textit{mm}$$

Each electrode was assumed to lie next to the lateral wall and Equation 3 in Escudé et al. (2006) was used to estimate an individual insertion angle:

$$\textit{Insertion angle} = (\exp(L \div (\textit{cochlea diameter} \times 2.62)) - 1) \times 235\ \textit{degrees}.$$

For Cochlear recipients, the insertion angle range was 51–76 and 370–670°, and the mean insertion angle ± SD was 57.7 ± 3.2 and 440 ± 37°, for the most basal and apical electrodes, respectively. For Med-El, the corresponding insertion angles were 50–62, 420–580, 55.7 ± 2.4, and 494 ± 32°.

2.6. Statistics

For statistical analysis, the insertion depths were divided into 10 insertion angle categories. The lower limit of the first category was 50° and the spacing between each category was 50°. As an exception, to reach a sufficient number of subjects, the width of the most apical category was increased to 100° with an upper limit of 600°, as the modeling of Z_{eff} for the ear with the greatest insertion depth (670°) was considered unsuccessful. Also, the lower limit was chosen to include all electrodes in the analyses. The number of measurements in each insertion angle category is shown in Table 3 in Appendix.

Finally, the correlation coefficients (Pearson's *r*) between the effective EF's peak amplitudes, its 50% widths, and the eCAP thresholds were computed for ears implanted with Cochlear devices. A two-way analysis of variance (ANOVA) was used in MATLAB to analyze statistically the effect of cochlear diameter on Z_{eff} with cochlear diameter group and electrode contact as independent variables and Z_{eff} as a dependent variable. Also, a two-way ANOVA was conducted to evaluate the effect of CI manufacturer on the intracochlear EF using the EF recording method and insertion angle category as independent variables and the relative distribution of EF as a dependent variable. As Z_{eff} and U_{eff} were in different units, the EF_{eff} peaks were normalized by dividing the EF_{eff} peaks with the smallest peak value for each ear. The post-hoc analyses were corrected with the Tukey method.

3. Results

In this study, we investigated the characteristics of the intracochlear EF. Figure 2 presents the relationship between the modeled peak amplitude and 50% width of the effective intracochlear EF. In Figure 2A, Z_{eff} is plotted against TIM_{eff} 50% width. There appears to be a linear correlation between the two ($r = 0.46$, $p < 0.001$), indicating that intracochlear EFs with high peak amplitudes are also wide along the scala tympani (ST). When the means of the Z_{eff} and TIM_{eff} 50% width are plotted at individual electrode contacts (Figure 2B), there is a clear relationship between the peak and width of the intracochlear EF in all the other regions but the most apical section of the electrode array.

Figure 3 illustrates the comparison of Z_{eff} and TIM_{eff} 50% width with the corresponding eCAP thresholds. In Figure 3A, Z_{eff} is plotted against eCAP thresholds. The eCAP thresholds decrease with the increase of Z_{eff} ($r = –0.41$, $p < 0.001$), demonstrating that when the current injected in the EF measurement generates a high local electric potential at the stimulating electrode, the current needed to elicit a measurable neural response in the eCAP measurement is low at the corresponding electrode.

Figure 3B shows the mean eCAP thresholds and Z_{eff} at individual electrode contacts. The mean eCAP threshold increases and the mean Z_{eff} decreases from the apical to basal direction along the electrode array ($r = 0.86$ and $r = –0.97$, respectively, $p < 0.001$ for both), suggesting that the two are inversely correlated. In Figure 3C, TIM_{eff} 50% width is plotted against the corresponding eCAP thresholds. Wide intracochlear EFs are associated with low eCAP thresholds ($r = –0.29$, $p < 0.001$), indicating that when a wide-spreading intracochlear EF is present in the EF measurement, less current is required to evoke a neural response in the eCAP measurement at the same electrode contact. When the mean eCAP thresholds and TIM_{eff} 50% widths are plotted at individual electrode contacts (Figure 3D), an increase of eCAP thresholds and TIM_{eff} 50% widths are seen in the apical section of the electrode array. However, from the middle to basal section of the electrode array their correlation seems to be inverse.

In order to study the effect of cochlear diameter on Z_{eff}, the cochleae were divided into four cochlear diameter groups (1–4 from smallest to

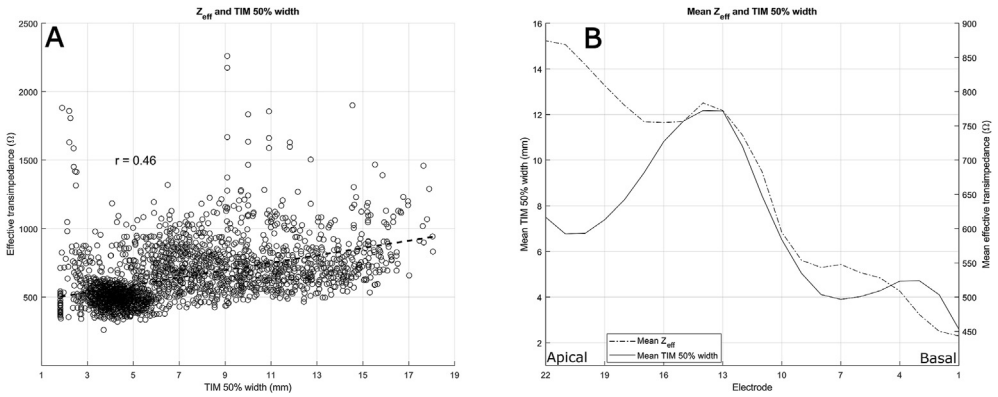

Figure 2. The relationship between the modeled peak transimpedance (Z_{eff}) and TIM_{eff} 50% width. A) The gapped line depicts linear regression between Z_{eff} and TIM_{eff} 50% width with corresponding Pearson's correlation coefficient ($r = 0.46$, $p < 0.001$). B) The means of Z_{eff} and TIM_{eff} 50% width plotted at individual electrode contacts from apical to basal direction.

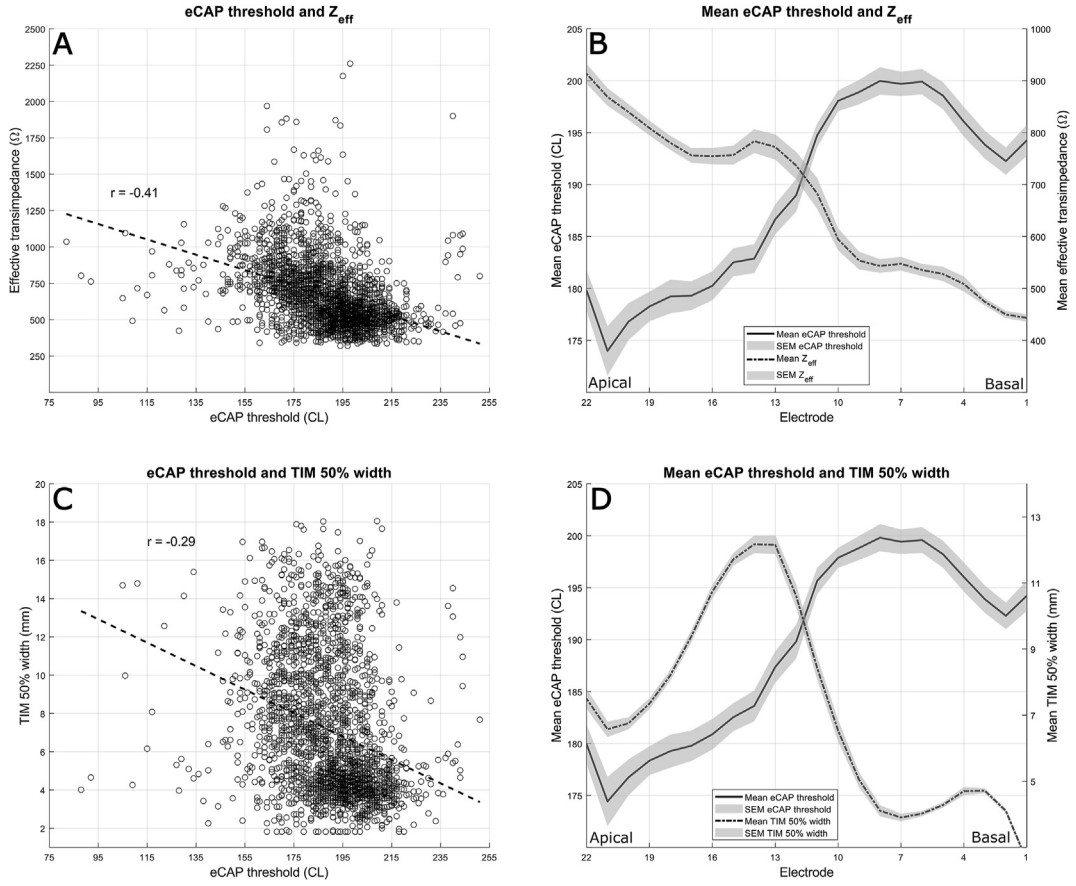

Figure 3. The relationships between the modeled peak amplitude (Z_{eff}) and width (TIM_{eff} 50% width) recorded via TIM with eCAP thresholds recorded via AutoNRT. A) Z_{eff} plotted against eCAP thresholds. The gapped line depicts linear regression ($r = –0.41$, $p < 0.001$). B) The means ± standard error of the means (SEM) of Z_{eff} and eCAP thresholds plotted at individual electrode contacts, which are plotted from the apical to basal direction. C) TIM_{eff} 50% width plotted against eCAP thresholds. The gapped line depicts linear regression ($r = –0.29$, $p < 0.001$). D) The means of Z_{eff} and eCAP thresholds plotted at individual electrode contacts.

largest, respectively, Figure 4A.) The peak amplitude of the intracochlear EF field is generally lower in the group with the largest cochleae, which was confirmed with a two-way ANOVA revealing a significant main effect of cochlear diameter group ($F(3, 2475) = 10.6$, $p < 0.001$). The mean ± SEM Z_{eff} was 650 ± 12, 670 ± 7.9, 681 ± 7.6, and 596 ± 11 Ω, for groups 1–4 (from smallest to largest), respectively. A pair-wise comparison after a post-hoc correction with the Tukey method revealed no significant differences in Z_{eff} between the groups 1–3 ($p = 0.57$, $p = 0.17$, and $p = 0.77$ for comparisons between group 1 vs 2, 1 vs 3, and 2 vs 3, respectively). However, the mean Z_{eff} of the group with the largest cochleae was lower than in the rest of the groups ($p < 0.05$ for all), indicating that the effect of cochlear diameter may become only apparent after a certain threshold.

To investigate Cochlear and Med-El devices with different electrode array designs and a different number of active electrode contacts, we plotted the Z_{eff} and U_{eff} against the insertion angle rather than electrode number. This also allowed us to consider the effect of different cochlea sizes detected in Figure 3. As seen in Figure 4B, the mean U_{eff} remains

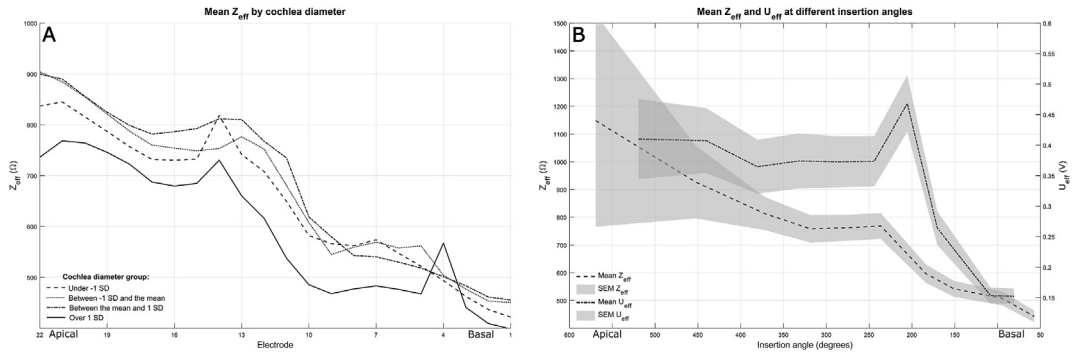

Figure 4. The mean Z_{eff} of groups sorted by cochlear diameter at different electrode contacts as well as a comparison of Z_{eff} and U_{eff}. A) The mean Z_{eff} is found from the y-axis and electrode contact from the x-axis B) The means of Z_{eff} and U_{eff} are plotted at the mean insertion angle of each insertion angle category.

relatively constant between insertion angles of 250–600° and then rapidly decreases, while Z_{eff} decreases more gradually towards the base of the cochlea. When the effect of the electrode location and the manufacturer on the relative distribution of the intracochlear EF was analyzed with a two-way ANOVA, there were significant main effects of insertion angle category and manufacturer, as well as an interaction between the two main effects ($F(10,3285) = 140$, $F(1,3285) = 332$, and $F(10, 3285) = 35.5$, respectively, $p < 0.001$ for all). In the post-hoc analyses, when the insertion angle was between 50–99 or 450–600, the relative distribution of EF_{eff} peaks were similar between the manufacturers. Between insertion angles of 100–449°, the relative EF_{eff} peaks were greater for Med-El than for Cochlear devices ($p < 0.001$ for all). However, when the correlation between the mean EF peak and the mean insertion angle of each insertion angle category was calculated, a general trend of lower EF peaks towards the base is apparent for both Cochlear ($r = 0.98$, $p < 0.001$) and Med-El ($r = 0.77$, $p = 0.01$).

In Figure 5, the major finding of the present study is summarized with a sketch of the ST. Electrode insertion depth is plotted categorically as an estimated insertion angle along with the corresponding mean Z_{eff} and eCAP threshold for the Slim Straight electrode array. In the basal part of the electrode array with a shallow insertion depth, the intracochlear EF (i.e., mean Z_{eff}) is low, and a high electrical current (in CL) is required to elicit a neural response. When moving along the electrode array towards to apex, the mean Z_{eff} increases while the eCAP threshold decreases, and there is a significant negative correlation between the two ($r = -0.95$, $p < 0.001$).

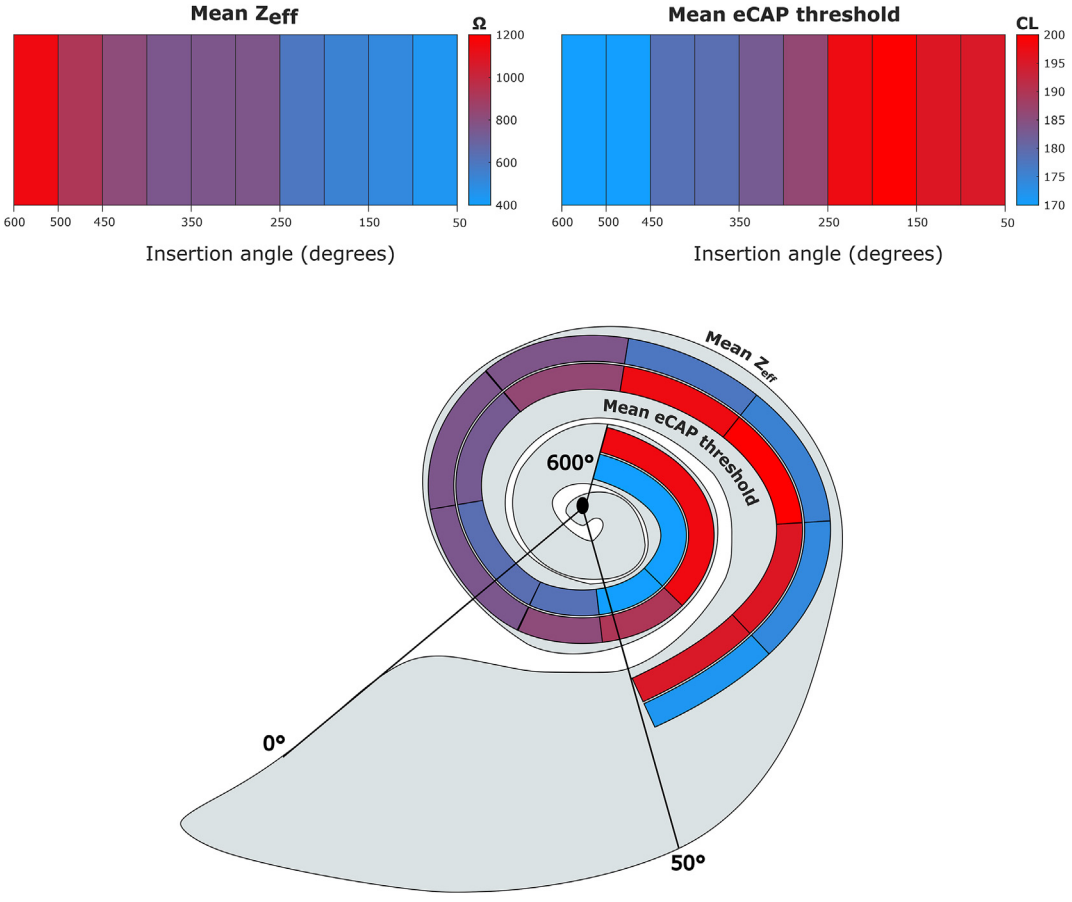

Figure 5. The mean Z_{eff} and eCAP thresholds at different insertion angles in the scala tympani. In complete insertion, the linear distance of the most basal electrode is 5 mm from the round window. The insertion angle range is 50–600°, and each cell covers 50° with an exception for the most apical cell, which covers 100°.

4. Discussion

The aim of this study was to investigate the relationship between the electrode-generated intracochlear EF and the excitability of the CN. We also assessed how the peak of the intracochlear EF is affected by the cochlear diameter, which is assumed to correlate with the modiolar distance of lateral-wall electrodes and ST diameter (Hatsushika et al., 1990; Escudé et al., 2006). The ST is the desired location of the electrode array and is bordered by the basilar membrane and bone, which are poorly conductive essentially confining the electrode-generated EF in the intrascalar space (Briaire and Frijns, 2000). Therefore, it was expected that high-peaked intracochlear EFs are generally wide-spreading. However, this is not true in the apex, where TIM 50% width decrease while Z_{eff} increase. This may be due to the scarcity of data apically to the recording electrode, which may lead to a narrower TIM 50% width, as the width will be determined mostly by the basal part of the EF peak. In addition to computational inaccuracies, there may be current paths across the turns of the cochlea which may explain the discrepancy between TIM 50% width and Z_{eff} in the apical part of the electrode array (Briaire and Frijns, 2006).

The inverse relationship between TIM_{eff} and eCAP thresholds as well as the lower Z_{eff} in larger than in smaller cochleae suggest that the neural excitability to electrical stimulation is dependent on the physical environment of the electrode array e.g., modiolar distance and scalar diameter. A previous modeling study found a sigmoid relationship between bone density and shallower decay of the intracochlear EF (Malherbe et al., 2015). Thus, high stimulation levels in conditions decreasing bone density, such as otosclerosis (Grayeli et al., 2004), may be required for sufficient loudness.

Generally, when the stimulation level is constant, the peak amplitudes of the generated intracochlear EFs increase towards the apex. A possible explanation for low peak amplitudes in the base is the current outflow from the round window, which may also be the cause of a narrow TIM 50% width in the basal part of the ST (see Figure 3D). Based on our unpublished study, in which temporal bones were implanted with Slim Straight electrodes and cochlear dimensions were measured, the scala area decreases towards the apical end of the ST in line with Biedron et al. (2010). Thus, the local potential generated by a stimulated electrode might be greater in narrow than in larger ST due to the better conductivity of the perilymph than of the conductivity of the bone (Briaire and Frijns, 2000). Unfortunately, due to the lack of post-operative imaging in our patient cohort, the exact placement of the electrode arrays in the ST is unknown.

Contrary to an earlier study, where intracochlear EF recordings were similar between different manufacturers (Swaddiwudhipong et al., 2020), in our study the modeled EFs were different between Cochlear and Med-El devices. As the modeling function utilizes EF recordings from non-stimulating electrodes, a greater amount of recording electrodes likely leads to a more accurate estimate of the effective EF. Even though the distribution of the effective EF was different between the manufacturers, the general trend of increasing EF peak amplitude was apparent for both Cochlear and Med-El devices. As earlier studies have found that eCAP thresholds tend to decrease towards the apex also with Med-El CIs (Brill et al., 2009; Estienne et al., 2021), a similar relationship between the EF and eCAP thresholds likely could be found with Med-El as with Cochlear devices. However, future studies are warranted to confirm this assumption.

Finally, combining knowledge of individual cochlear anatomy, the properties of the intracochlear EF, and the responsiveness of the auditory nerve to electrical stimulation with audiometric measures will most likely result in more predictable CI outcomes, irrespective of the device brand. Although the exact electrode location was not available in this study due to the lack of postoperative imaging, the results highlight that the intracochlear EF and eCAP thresholds are linked and to some extent dependent on cochlear size in the intraoperative setting. This may help set the initial stimulation levels in cases with absent neural responses based on other individual measures, such as anatomy and the properties of the intracochlear EF. However, the eCAP thresholds tend to decrease within the first months after activation of the CI (Molisz et al., 2015) and thus, further studies investigating the eCAP thresholds and intracochlear EF in post-operative settings are warranted.

5. Conclusion

Intracochlear EFs with high peak amplitudes tend to spread widely along the ST. When the stimulating current generates an EF with a high and wide peak amplitude in EF measurements, less current is needed to excite the auditory nerve in eCAP measurements in the corresponding electrodes. The peak amplitude of the intracochlear EF is higher in the apex than in the base, and similar stimulation levels cause weaker EFs in larger than in smaller cochleae. The results suggest that the neural excitability to electrical stimulation is dependent on the physical environment of the electrode array, such as the dimensions of the cochleae.

Declarations

Author contribution statement

Samuel Söderqvist, M.D; Saku T. Sinkkonen; Ville Sivonen: Conceived and designed the experiments; Performed the experiments; Analyzed and interpreted the data; Contributed reagents, materials, analysis tools or data; Wrote the paper.

Funding statement

This research did not receive any specific grant from funding agencies in the public, commercial, or not-for-profit sectors. Open access was funded by Helsinki University Library.

Data availability statement

Data included in article/supp. material/referenced in article.

Declaration of interest's statement

The authors declare no conflict of interest.

Additional information

No additional information is available for this paper.

Appendix

Table 1. The patient demographics. If both ears from a single patient were included in the study, the right ear is marked with an "R" and left with an "L".

Patients with Cochlear C522 and C622 with Slim Straight electrode array				
ID	Cochlear diameter (mm)	Age	Ear	Hearing loss etiology
1	8.10	44.8	Right	Unknown
2R	9.0	42.1	Right	Unknown
2L	9.8	44.0	Left	Unknown
3	9.2	21.6	Right	Unknown
4	8.6	53.8	Left	Unknown
5	9.0	57.3	Right	Unknown
6	9.0	37.8	Left	Unknown
7	8.7	50.8	Left	Unknown
8R	8.6	45.7	Left	Unknown
8L	8.5	46.4	Right	Unknown
9	8.1	82.0	Right	Unknown
10	7.9	4.7	Left	Unknown
11	-	16.9	Right	Unknown
12R	9.3	0.8	Right	Unknown
12L	9.3	0.8	Left	Unknown
13	9.1	6.5	Right	Unknown
14R	9.3	0.7	Right	Connexin-mutation
14L	9.0	0.7	Left	Connexin-mutation
15	8.5	15.1	Left	Unknown
16	8.4	64.3	Right	Unknown
17	8.7	58.9	Right	Unknown
18	8.7	39.7	Left	Unknown
19	8.6	24.8	Right	Unknown
20	8.5	45.6	Right	Unknown
21	8.0	60.5	Left	Unknown
22	9.0	47.1	Left	Unknown
23	8.4	41.9	Left	Unknown
24R	8.3	47.1	Right	Unknown
24L	8.6	45.6	Left	Unknown
25	9.0	35.4	Right	Meningitis
26	8.6	78.9	Left	Meniere
27R	8.9	3.8	Right	Unknown
27L	8.9	3.8	Left	Unknown
28	8.5	5.5	Left	Unknown
29	8.7	2.2	Right	Unknown
30	8.5	11.7	Right	Unknown
31	8.4	3.9	Right	Unknown
32	8.9	5.4	Right	Connexin
33	8.2	23.1	Right	Unknown
34	9.2	52.9	Right	Maternal rubella
35	8.1	56.0	Left	Usher
36	8.7	57.0	Left	Unknown
37	-	75.7	Left	Unknown
38	8.9	58.3	Right	Unknown
39	8.9	14.2	Left	Unknown
40	8.2	10.6	Right	Unknown
41R	8.8	0.8	Right	Unknown
41L	9.1	0.8	Left	Unknown
42R	8.9	1.1	Right	Maternal CMV
42L	8.9	1.1	Left	Maternal CMV
43	7.7	1.3	Right	Cochlear nerve hypoplasia
44	9.1	4.4	Left	Unknown
45R	8.5	1.0	Right	Unknown
45L	8.7	1.0	Left	Unknown
46R	8.9	1.1	Right	Unknown
46L	9.1	1.1	Left	Unknown

(*continued on next page*)

Table 1 (*continued*)

Patients with Cochlear C522 and C622 with Slim Straight electrode array				
ID	Cochlear diameter (mm)	Age	Ear	Hearing loss etiology
47R	8.9	0.9	Right	Unknown
47L	8.8	0.9	Left	Unknown
48R	8.5	0.8	Right	Unknown
48L	8.6	0.8	Left	Unknown
49R	8.8	12.6	Right	Asphyxia
49L	8.8	13.6	Left	Unknown
50	6.8	17.3	Right	Unknown
51R	9.5	0.9	Right	Unknown
51L	9.5	0.9	Left	Unknown
52	8.9	27.5	Left	Unknown
53	9.4	50.7	Right	Unknown
54R	8.7	46.0	Left	Otosclerosis
54L	8.7	45.7	Left	Otosclerosis
55	8.9	38.7	Left	Meniere
56	8.9	60.5	Left	Unknown
57	8.8	42.2	Left	Unknown
58	8.6	54.5	Left	Unknown
59R	8.4	50.7	Right	Otosclerosis
59L	9.0	50.4	Left	Otosclerosis
60	9.0	60.1	Right	Unknown
61R	8.5	54.8	Right	Unknown
61L	8.5	55.5	Left	Unknown
62	8.0	49.0	Right	Unknown
63	8.7	36.2	Right	Meningitis
64	8.9	55.6	Right	Unknown
65	8.7	32.8	Left	Meniere
66	8.7	78.3	Left	Unknown
67	9.0	77.9	Left	Unknown
68	9.1	53.3	Left	Otosclerosis
69	8.5	55.0	Left	Unknown
70	8.6	42.1	Right	Unknown
71	8.5	66.6	Left	Unknown
72	8.8	25.8	Right	Unknown
73	8.7	67.0	Right	Unknown
74	9.0	50.8	Left	Otosclerosis
75	8.9	25.1	Left	Unknown
76	9.2	89.9	Right	Chronic otitis media
77	8.9	34.4	Left	Unknown
78	8.2	68.2	Left	Unknown
79	9.3	71.4	Left	Unknown
80	9.0	69.1	Left	Unknown
81	8.0	54.1	Right	Preterm birth
82	9.1	74.3	Left	Meniere
83	9.2	57.9	Right	Meniere
85	9.3	74.2	Right	Unknown
86	9.3	35.2	Left	Renal insufficiency
87	8.7	34.7	Left	Unknown
88	8.8	66.5	Right	Unknown
89R	8.4	0.9	Right	Connexin-mutation
89L	8.5	0.9	Left	Connexin-mutation
90R	8.4	2.0	Right	Unknown
90L	8.4	2.0	Left	Unknown
91R	8.5	0.9	Right	Unknown
91L	8.5	0.9	Left	Unknown
92R	8.8	3.9	Right	Unknown
92L	9.1	3.9	Left	Unknown
93	9.1	5.3	Right	Unknown
94R	8.2	1.2	Right	Unknown

(*continued on next page*)

Table 1 (*continued*)

Patients with Cochlear C522 and C622 with Slim Straight electrode array				
ID	Cochlear diameter (mm)	Age	Ear	Hearing loss etiology
94L	8.4	1.2	Left	Unknown
95R	8.6	2.4	Right	Unknown
95L	8.6	2.4	Left	Unknown
96L	8.2	1.0	Right	Unknown
96R	8.2	1.0	Left	Unknown
Patients with Med-El Synchrony with Flex 28 electrode array				
ID	Cochlear diameter (mm)	Age	Ear	Hearing loss etiology
1	8.3	83.7	Right	Presbycusis
2	8.8	74.2	Right	Unknown
3	8.8	75.0	Right	Meningitis
4	8.9	77.7	Right	Meniere
5	8.8	78.0	Left	Sudden deafness
6	8.6	25.8	Left	Unknown
7R	8.5	58.3	Right	Unknown
7L	8.8	54.6	Left	Unknown
8	9.7	81.6	Left	Sudden deafness
9	8.7	73.8	Right	Unknown
10	8.7	84.2	Left	Unknown
11	8.8	57.4	Left	Usher
12	8.2	83.0	Right	Unknown
13	8.9	63.4	Left	Unknown
14	8.9	46.4	Right	Unknown
15	8.9	83.5	Right	Sudden deafness
16	8.9	76.5	Right	Unknown
17	8.5	72.5	Left	Cochlear nerve aplasia
18	9.6	61.1	Right	Unknown
19	9.1	76.4	Right	Unknown
20	9.4	70.1	Right	Unknown
21	8.5	56.5	Right	Unknown
22	8.4	77.8	Right	Unknown
23	8.0	51.9	Left	Unknown
24R	8.7	32.5	Right	Unknown
24L	8.8	34.7	Left	Unknown
25	8.9	59.5	Right	Unknown
26	8.7	84.1	Left	Unknown
27	9.4	53.4	Right	Unknown
28	9.0	83.8	Left	Unknown
29	8.3	67.0	Right	Unknown
30	8.6	76.0	Left	Unknown
31	8.6	27.3	Left	Unknown
32	9.1	64.1	Right	Unknown
33	9.3	50.3	Right	Unknown
34	8.4	73.9	Left	Unknown
35	9.5	79.0	Right	Unknown
36	8.7	41.7	Right	Unknown
37	8.6	67.6	Left	Otosclerosis
38	8.2	74.8	Right	Unknown
39	9.1	72.7	Right	Unknown
40	8.5	35.6	Left	Unknown
41	8.5	65.6	Left	Meniere
42	8.8	74.6	Left	Unknown
43	8.4	74.8	Right	Unknown
44	8.6	80.5	Right	Unknown
45	8.6	45.2	Right	Unknown
46	8.9	42.4	Right	Usher
47	8.9	50.0	Right	Usher
48R	8.4	56.1	Right	Meniere
48L	8.5	54.3	Left	Meniere

(*continued on next page*)

Table 1 (*continued*)

Patients with Med-El Synchrony with Flex 28 electrode array				
ID	Cochlear diameter (mm)	Age	Ear	Hearing loss etiology
49	9.0	59.9	Left	Unknown
50	8.8	68.0	Right	Unknown
51	8.9	75.0	Left	Unknown
52	8.9	39.0	Left	Unknown
53	9.3	40.7	Right	Unknown
54	9.2	21.4	Left	Unknown
55	9.1	58.8	Right	Unknown
56	9.2	56.3	Left	Unknown
57	8.9	39.1	Left	Unknown
58	9.3	23.9	Left	Meningitis
59	8.6	35.5	Right	Meningitis
60	9.2	49.8	Right	Unknown
61	8.5	75.0	Right	Meniere
62	8.8	76.2	Left	Unknown
63	8.9	66.6	Left	Unknown
64	8.8	48.9	Left	Usher
65	8.6	62.4	Left	Unknown
66	8.8	69.6	Left	Sudden deafness
67	8.3	68.7	Left	Unknown
68	9.6	71.8	Right	Meniere
69	9.0	85.1	Left	Unknown
70	-	17.7	Left	Unknown
71	8.9	3.4	Left	Connexin mutation

Table 2. The number of available TIM_{eff} and IFT_{eff} from each electrode contact. For TIM_{eff}, the corresponding 50% widths and eCAP thresholds are also shown. The electrodes are arranged from the apical to basal direction, which is from 22 to 1 in Cochlear devices and the opposite in Med-El devices.

Cochlear C522 and C622 with Slim Straight electrode array								
Electrode	22	21	20	19	18	17	16	15
Zeff	98 %	98 %	97 %	98 %	97 %	96 %	96 %	96 %
NRT	96 %	97 %	96 %	97 %	97 %	97 %	97 %	95 %
Both	94 %	95 %	94 %	96 %	94 %	94 %	94 %	92 %
Electrode	14	13	12	11	10	9	8	
Zeff	96 %	95 %	96 %	96 %	96 %	97 %	96 %	
NRT	95 %	96 %	98 %	98 %	98 %	98 %	97 %	
Both	92 %	92 %	94 %	94 %	94 %	96 %	94 %	
Electrode	7	6	5	4	3	2	1	
Zeff	96 %	96 %	96 %	96 %	96 %	95 %	94 %	
NRT	97 %	97 %	97 %	97 %	96 %	97 %	98 %	
Both	94 %	92 %	94 %	93 %	92 %	93 %	93 %	
Med-El Synchrony with Flex 28 electrode array								
Electrode	1	2	3	4	5	6		
IFTeff	86 %	89 %	91 %	88 %	73 %	53 %		
IFT_{eff} 50% width	0 %	35 %	65 %	62 %	50 %	23 %		
Electrode	7	8	9	10	11	12		
IFTeff	36 %	69 %	88 %	97 %	97 %	96 %		
IFT_{eff} 50% width	16 %	34 %	50 %	55 %	69 %	0 %		

Table 3. The number of available Z_{eff} and U_{eff} in each insertion angle category.

Insertion angle	50–99	100–149	150–199	200–249	250–299	300–349	350–399	400–449	450–499	500–600
Zeff count	461	410	355	328	274	264	235	186	50	9
Ueff count	151	137	94	104	87	78	71	65	59	30

References

Alexiades, G., Dhanasingh, A., Jolly, C., 2015. Method to estimate the complete and two-turn cochlear duct length. Otol. Neurotol. 36, 904–907.

Bai, S., Encke, J., Obando-Leitón, M., Weiß, R., Schäfer, F., Eberharter, J., Böhnke, F., Hemmert, W., 2019. Electrical stimulation in the human cochlea: a computational study based on high-resolution micro-CT scans. Front. Neurosci. 13, 1312.

Berenstein, C.K., Vanpoucke, F.J., Mulder, J.J.S., Mens, L.H.M., 2010. Electrical field imaging as a means to predict the loudness of monopolar and tripolar stimuli in cochlear implant patients. Hear. Res. 270, 28–38.
Biedron, S., Prescher, A., Ilgner, J., Westhofen, M., 2010. The internal dimensions of the cochlear scalae with special reference to cochlear electrode insertion trauma. Otol. Neurotol. 31, 731–737.
Briaire, J.J., Frijns, J.H.M., 2006. The consequences of neural degeneration regarding optimal cochlear implant position in scala tympani: a model approach. Hear. Res. 214, 17–27.
Briaire, J.J., Frijns, J.H.M., 2000. Field patterns in a 3D tapered spiral model of the electrically stimulated cochlea. Hear. Res. 148, 18–30.
Brill, S., Müller, J., Hagen, R., Möltner, A., Brockmeier, S.-J., Stark, T., Helbig, S., Maurer, J., Zahnert, T., Zierhofer, C., Nopp, P., Anderson, I., Strahl, S., 2009. Site of cochlear stimulation and its effect on electrically evoked compound action potentials using the MED-EL standard electrode array. Biomed. Eng. Online 8, 40.
Cafarelli Dees, D., Dillier, N., Lai, W.K., von Wallenberg, E., van Dijk, B., Akdas, F., Aksit, M., Batman, C., Beynon, A., Burdo, S., Chanal, J.-M., Collet, L., Conway, M., Coudert, C., Craddock, L., Cullington, H., Deggouj, N., Fraysse, B., Grabel, S., Kiefer, J., Kiss, J.G., Lenarz, T., Mair, A., Maune, S., Müller-Deile, J., Piron, J.-P., Razza, S., Tasche, C., Thai-Van, H., Toth, F., Truy, E., Uziel, A., Smoorenburg, G.F., 2005. Normative findings of electrically evoked compound action potential measurements using the neural response telemetry of the Nucleus CI24M cochlear implant system. Audiol. Neurotol. 10, 105–116.
Christov, F., Gluth, M.B., Hans, S., Lang, S., Arweiler-Harbeck, D., 2019. Impact of cochlear tonotopy on electrically evoked compound action potentials (ECAPs). Acta Otolaryngol. 139, 22–26.
Cohen, L.T., Richardson, L.M., Saunders, E., Cowan, R.S.C., 2003. Spatial spread of neural excitation in cochlear implant recipients: comparison of improved ECAP method and psychophysical forward masking. Hear. Res. 179, 72–87.
Colesa, D.J., Devare, J., Swiderski, D.L., Beyer, L.A., Raphael, Y., Pfingst, B.E., 2021. Development of a chronically-implanted mouse model for studies of cochlear health and implant function. Hear. Res. 404, 108216.
Cooper, T., Melder, K.L., Hyre, R., Hobson, C.E., McCall, A.A., Hirsch, B.E., 2020. Cochlear implant performance in adult patients with absent intraoperative electrically evoked compound action potentials. Otolaryngol. Neck Surg. 162, 725–730.
Davis, T.J., Zhang, D., Gifford, R.H., Dawant, B.M., Labadie, R.F., Noble, J.H., 2016. Relationship between electrode-to-Modiolus distance and current levels for adults with cochlear implants. Otol. Neurotol. 37, 31–37.
de Rijk, S.R., Tam, Y.C., Carlyon, R.P., Bance, M.L., 2020 Sep/Oct. Detection of extracochlear electrodes in cochlear implants with electric field imaging/transimpedance measurements: a human cadaver study. Ear Hear. 41 (5), 1196–1207.
Dietz, A., Wennström, M., Lehtimäki, A., Löppönen, H., Valtonen, H., 2016. Electrode migration after cochlear implant surgery: more common than expected? Eur. Arch. Oto-Rhino-Laryngol. 273, 1411–1418.
Dorman, M.F., Gifford, R.H., 2017. Speech understanding in complex listening environments by listeners fit with cochlear implants. J. Speech Lang. Hear. Res. 60, 3019–3026.
Durisin, M., Büchner, A., Lesinski-Schiedat, A., Bartling, S., Warnecke, A., Lenarz, T., 2015. Cochlear implantation in children with bacterial meningitic deafness: the influence of the degree of ossification and obliteration on impedance and charge of the implant. Cochlear Implants Int. 16, 147–158.
Escudé, B., James, C., Deguine, O., Cochard, N., Eter, E., Fraysse, B., 2006. The size of the cochlea and predictions of insertion depth angles for cochlear implant electrodes. Audiol. Neurotol. 11, 27–33.
Estienne, P., Scaglia, A., Kontides, A., Lauss, K., Schwarz, K., Arauz, S.L., 2021. Comparison of automated and traditional ECAP recording approaches in clinical practice. Int. J. Audiol. 1–9.
Friesen, L.M., Shannon, R.V., Baskent, D., Wang, X., 2001. Speech recognition in noise as a function of the number of spectral channels: comparison of acoustic hearing and cochlear implants. J. Acoust. Soc. Am. 110, 1150–1163.
Grayeli, A.B., Yrieix, C.S., Imauchi, Y., Cyna-gorse, F., Ferrary, E., Sterkers, O., 2004. Temporal bone density measurements using CT in otosclerosis. Acta Otolaryngol. 124, 1136–1140.
Hatsushika, S.-I., Shepherd, R.K., Tong, Y.C., Clark, G.M., Funasaka, S., 1990. Dimensions of the scala tympani in the human and cat with reference to cochlear implants. Ann. Otol. Rhinol. Laryngol. 99, 871–876.
Helmstaedter, V., Buechner, A., Stolle, S., Goetz, F., Lenarz, T., Durisin, M., 2018. Cochlear implantation in children with meningitis related deafness: the influence of electrode impedance and implant charge on auditory performance – a case control study. Int. J. Pediatr. Otorhinolaryngol. 113, 102–109.
Hey, M., Böhnke, B., Dillier, N., Hoppe, U., Eskilsson, G., Löwgren, K., Cullington, H., Mauch, H., Müller-Deile, J., 2015. The Intra-Cochlear Impedance-Matrix (IIM) test for the Nucleus® cochlear implant. Biomed. Eng. Biomed. Tech. 60.
Hoppe, U., Brademann, G., Stöver, T., Ramos de Miguel, A., Cowan, R., Manrique, M., Falcón-González, J.C., Hey, M., Baumann, U., Huarte, A., Liebscher, T., Bennett, C., English, R., Neben, N., Ramos Macías, A., 2022. Evaluation of a transimpedance matrix algorithm to detect anomalous cochlear implant electrode position. Audiol. Neurotol. 1–9.
Hughes, M.L., Brown, C.J., Abbas, P.J., 2004. Sensitivity and specificity of averaged electrode voltage measures in cochlear implant recipients. Ear Hear. 25, 431–446.
Jahn, K.N., Arenberg, J.G., 2020. Electrophysiological estimates of the electrode–neuron interface differ between younger and older listeners with cochlear implants. Ear Hear. 41, 948–960.
Jeon, E.K., Brown, C.J., Etler, C.P., O'Brien, S., Chiou, L.-K., Abbas, P.J., 2010. Comparison of electrically evoked compound action potential thresholds and loudness estimates for the stimuli used to program the advanced Bionics cochlear implant. J. Am. Acad. Audiol. 21, 16–27.
Kirby, B., Brown, C., Abbas, P., Etler, C., O'Brien, S., 2012. Relationships between electrically evoked potentials and loudness growth in bilateral cochlear implant users. Ear Hear. 33, 389–398.
Lai, W.K., Dillier, N., 2000. A simple two-component model of the electrically evoked compound action potential in the human cochlea. Audiol. Neurotol. 5, 333–345.
Lai, W.K., Müller-Deile, J., Dillier, N., Almqvist, B., Stecker, M., Frohne, C., von Wallenberg, E., 2002. Measurement of the electrically evoked compound action potential via a neural response telemetry system. Ann. Otol. Rhinol. Laryngol. 111, 407–414.
Landsberger, D.M., Padilla, M., Srinivasan, A.G., 2012. Reducing current spread using current focusing in cochlear implant users. Hear. Res. 284, 16–24.
Lei, I.M., Jiang, C., Lei, C.L., de Rijk, S.R., Tam, Y.C., Swords, C., Sutcliffe, M.P.F., Malliaras, G.G., Bance, M., Huang, Y.Y.S., 2021. 3D printed biomimetic cochleae and machine learning co-modelling provides clinical informatics for cochlear implant patients. Nat. Commun. 12, 6260.
Long, C.J., Holden, T.A., McClelland, G.H., Parkinson, W.S., Shelton, C., Kelsall, D.C., Smith, Z.M., 2014. Examining the electro-neural interface of cochlear implant users using psychophysics, CT scans, and speech understanding. J. Assoc. Res. Otolaryngol. 15, 293–304.
Luo, X., Wu, C.-C., 2016. Symmetric electrode spanning narrows the excitation patterns of partial tripolar stimuli in cochlear implants. J. Assoc. Res. Otolaryngol. 17, 609–619.
Malherbe, T.K., Hanekom, T., Hanekom, J.J., 2015. The effect of the resistive properties of bone on neural excitation and electric fields in cochlear implant models. Hear. Res. 327, 126–135.
Mewes, A., Brademann, G., Hey, M., 2020. Comparison of perimodiolar electrodes: imaging and electrophysiological outcomes. Otol. Neurotol. 41, e934–e944.
Miller, C.A., Brown, C.J., Abbas, P.J., Chi, S.-L., 2008. The clinical application of potentials evoked from the peripheral auditory system. Hear. Res. 242, 184–197.
Molisz, A., Zarowski, A., Vermeiren, A., Theunen, T., De Coninck, L., Siebert, J., Offeciers, E.F., 2015. Postimplantation changes of electrophysiological parameters in patients with cochlear implants. Audiol. Neurotol. 20, 222–228.
Morita, T., Naito, Y., Hirai, T., Yamaguchi, S., Ito, J., 2003. The relationship between the intraoperative ECAP threshold and postoperative behavioral levels: the difference between postlingually deafened adults and prelingually deafened pediatric cochlear implant users. Eur. Arch. Oto-Rhino-Laryngol. 260, 67–72.
Morris, D.J.E., Pfingst, B., 2000. Effects of electrode configuration and stimulus level on rate and level discrimination with cochlear implants. J. Assoc. Res. Otolaryngol. 1, 211–223.
Newbold, C., Richardson, R., Millard, R., Seligman, P., Cowan, R., Shepherd, R., 2011. Electrical stimulation causes rapid changes in electrode impedance of cell-covered electrodes. J. Neural. Eng. 8, 036029.
Nogueira, W., Schurzig, D., Büchner, A., Penninger, R.T., Würfel, W., 2016. Validation of a cochlear implant patient-specific model of the voltage distribution in a clinical setting. Front. Bioeng. Biotechnol. 4.
Padilla, M., Landsberger, D.M., 2016. Reduction in spread of excitation from current focusing at multiple cochlear locations in cochlear implant users. Hear. Res. 333, 98–107.
Pfingst, B.E., Zhou, N., Colesa, D.J., Watts, M.M., Strahl, S.B., Garadat, S.N., Schvartz-Leyzac, K.C., Budenz, C.L., Raphael, Y., Zwolan, T.A., 2015. Importance of cochlear health for implant function. Hear. Res. 322, 77–88.
Schvartz-Leyzac, K.C., Holden, T.A., Zwolan, T.A., Arts, H.A., Firszt, J.B., Buswinka, C.J., Pfingst, B.E., 2020. Effects of electrode location on estimates of neural health in humans with cochlear implants. J. Assoc. Res. Otolaryngol. 21, 259–275.
Shepherd, R.K., Hatsushika, S., Clark, G.M., 1993. Electrical stimulation of the auditory nerve: the effect of electrode position on neural excitation. Hear. Res. 66, 108–120.
Snyder, R.L., Bierer, J.A., Middlebrooks, J.C., 2004. Topographic spread of inferior colliculus activation in response to acoustic and intracochlear electric stimulation. J. Assoc. Res. Otolaryngol. 5, 305–322.
Söderqvist, S., Lamminmäki, S., Aarnisalo, A., Hirvonen, T., Sinkkonen, S.T., Sivonen, V., 2021. Intraoperative transimpedance and spread of excitation profile correlations with a lateral-wall cochlear implant electrode array. Hear. Res. 405, 108235.
Söderqvist, S., Sivonen, V., Lamminmäki, S., Ylönen, J., Markkola, A., Sinkkonen, S.T., 2022. Investigating the association of electrically-evoked compound action potential thresholds with inner-ear dimensions in pediatric cochlear implantation. Int. J. Pediatr. Otorhinolaryngol. 158, 111160.
Srinivasan, A.G., Padilla, M., Shannon, R.V., Landsberger, D.M., 2013. Improving speech perception in noise with current focusing in cochlear implant users. Hear. Res. 299, 29–36.
Swaddiwudhipong, N., Jiang, C., Landry, T.G., Bance, M., 2020. Investigating the electrical properties of different cochlear implants. Otol. Neurotol.
Swiderski, D.L., Colesa, D.J., Hughes, A.P., Raphael, Y., Pfingst, B.E., 2020. Relationships between intrascalar tissue, neuron survival, and cochlear implant function. J. Assoc. Res. Otolaryngol. 21, 337–352.
Tang, Q., Benítez, R., Zeng, F.-G., 2011. Spatial channel interactions in cochlear implants. J. Neural. Eng. 8, 046029.
Telmesani, L.M., Said, N.M., 2015. Effect of cochlear implant electrode array design on auditory nerve and behavioral response in children. Int. J. Pediatr. Otorhinolaryngol. 79, 660–665.

van Wermeskerken, G.K.A., van Olphen, A.F., Graamans, K., 2009. Imaging of electrode position in relation to electrode functioning after cochlear implantation. Eur. Arch. Oto-Rhino-Laryngol. 266, 1527–1531.

Vanpoucke, F.J., Zarowski, A.J., Peeters, S.A., 2004. Identification of the impedance model of an implanted cochlear prosthesis from intracochlear potential measurements. IEEE Trans. Biomed. Eng. 51, 2174–2183.

Wilson, B.S., Finley, C.C., Lawson, D.T., Wolford, R.D., Eddington, D.K., Rabinowitz, W.M., 1991 Jul 18. Better speech recognition with cochlear implants. Nature 352 (6332), 236–238.

Zuniga, M.G., Rivas, A., Hedley-Williams, A., Gifford, R.H., Dwyer, R., Dawant, B.M., Sunderhaus, L.W., Hovis, K.L., Wanna, G.B., Noble, J.H., Labadie, R.F., 2017. Tip Fold-Over in cochlear implantation: case series. Otol. Neurotol. 38, 199–206.